Hindawi
International Journal of Antennas and Propagation
Volume 2022, Article ID 5684055, 10 pages
https://doi.org/10.1155/2022/5684055

Research Article

Wideband Circularly Polarized Microstrip-Slot Antenna with Parasitic Ground Planes

Qin Huang [1,2]

[1]*Institute of Semiconductors, Guangdong Academy of Science, Guangzhou, China*
[2]*Guangzhou Fastprint Circuit Tech Co., Ltd., Guangzhou, China*

Correspondence should be addressed to Qin Huang; yliu1987@foxmail.com

Received 22 September 2022; Revised 11 November 2022; Accepted 17 November 2022; Published 23 November 2022

Academic Editor: Trushit Upadhyaya

In this study, a new stacked microstrip slot antenna (MSA) with wideband circular polarization (CP) characteristics is proposed. The antenna consists of a square-loop feed configuration, four parasitic square patches, four parasitic vertical planes, and a square ground plane etched with four parasitic square slots. The corner-cut square-loop can excite a stable 270° phase difference by loading an arc-shaped strip into the square-loop. Square-patches, vertical planes, and square slots as parasitic elements are placed together at the side of the square-loop to stimulate two CP resonant points. Simulation and measurement are performed on the designed antenna prototype to demonstrate the design's rationality. The measured results depict that the measured impedance bandwidth (IBW) for $|S_{11}| < -10$ dB is 36.4% (4.65 to 6.70 GHz) and the measured axial ratio bandwidth (ARBW) for AR < 3 dB is 25.1% (5.01 to 6.45 GHz). Compared with other reported stacked CP antennas, the proposed antenna has significant advantages in CP bandwidth, which could occupy the wireless local area network ITS (5.8 GHz), (5.725–5.85 GHz), and WIFI (5.85–5.925 GHz) bands.

1. Introduction

Although linear polarization wideband antennas [1–7] are used in various wireless communication systems, circular polarization (CP) antennas have a stronger attraction in some communication systems due to the merits of suppressing multipath interference and reducing polarization misalignment [8–11]. In addition, with the development of high-rate transmission and processing systems, CP antennas with wide bandwidth, high gains, and low-profile characteristics are also in great demand [12–15].

Various CP antennas have been extensively designed to achieve wideband operation, such as microstrip patch antennas [13–15], dielectric resonator antennas [16], and cross-dipole antennas [17–19]. Currently, a pair of orthogonal vacant-quarter fabricated rings as sequentially-rotated feeding structures has been extensively used in the design of crossed-dipole CP antennas, which can provide a stable 90° phase difference to achieve CP operation. Based on the feeding structure, many different shapes of crossed-dipole antennas are presented to obtain broadband CP radiation [20–26]. These shapes of crossed-dipole involve liner [20], rectangular [21], stepped rectangular [22], metallic cuboids [23], *L*-shaped [24], elliptical [25], and asymmetric bowtie [26] cross-dipoles, which are designed in turn to obtain wide 15.6%, 27%, 55.1%, 86.4%, 67.5%, and 96.6% of 3-dB ARBW, respectively. However, the profile of the cross-dipole antenna is too high due to the presence of a quarter wavelength grounded reflector, which is not suitable for low-profile applications. CP microstrip patch antennas (MPAs) have a lower profile than cross-dipole antennas and have also been studied in recent years [27–34].

Recently, many sequential phase feeding structures, which could provide a stable sequential phase difference, have been often used in the design of CP MPAs. These sequential phase feeding structures could be summarized as: an aperture-coupled feeding structure [35], a coplanar-waveguide feeding structure [36], series-parallel feeding structures [13, 16], and square-loop feeding structures [15, 27–44]. Besides, the stacked technique [42–46] is also an

effective method for enhancing the CP bandwidth on the basis of the sequential phase feeding structures. Circular patch [43], rectangular patch [44], L-shaped patch [45], and square patch [46] are stacked above the sequential phase feeding structure as parasitic elements, which could realize 6%, 28.1%, 16.7%, and 19.4% CP bandwidth, respectively.

In contrast to the conventional parasitic patches, square slots and vertical grounded patches as parasitic elements are introduced into the design of the CP MPA in this study. The proposed antenna is comprised of a square-loop feed configuration, four parasitic square patches, four parasitic vertical planes, and a square ground plane etched with four parasitic square slots. By using these parasitic elements, two CP resonant points could be excited at the same time. Simulation and measurement are performed on the designed antenna prototype to demonstrate the design's rationality. The measured impedance bandwidth (IBW) for $|S_{11}| < -10$ dB is 36.4% (4.65 to 6.70 GHz) and the measured axial ratio bandwidth (ARBW) for AR < 3 dB is 25.1% (5.01 to 6.45 GHz).

2. Antenna Design

2.1. Antenna Configuration. Figure 1 shows the entire geometry and details of the wideband stacked CP MPA. As seen, the proposed MPA consists of a coaxially fed square-loop structure, four rotated square patches ($L1 \times W1 \times G1$), four rotated square slots ($L2 \times W2$), and four vertically grounded patches ($L3 \times W3$). The proposed MPA is fabricated on the Rogers 5880 substrate ($\varepsilon_r = 2.2$, $h = 1.524$ mm, and $\tan\delta = 0.001$). Note that the square-loop feeding structure is composed of an arc-shaped strip ($R0 \times R1$) with the angle of 270° and a length of $\lambda g/4$ (λg is the waveguide length at 5.5 GHz) and a square-loop ($D2 \times D3$) that is used to stimulate the fundamental one-wavelength mode [6]. By using these parasitic patches and slots, two CP resonant points could be stimulated at the same time, achieving a wide CP bandwidth. Moreover, four parasitic vertical planes are used to improve the CP bandwidth of the proposed antenna. At last, the optimized dimensions of the proposed MPA are summarized in Table 1 after using ANSYS HFSS to tune and optimize.

2.2. Antenna Mechanism. To demonstrate the design mechanism, four different step-by-step prototypes are investigated in Figure 2. For a clear comparison, the relevant $|S_{11}|$ and AR results are depicted in Figures 3(a) and 3(b). First, a conventional square-loop feeding structure with four parasitic square patches (Ant. 1); second, the square-loop feeding structure with four parasitic square slots (Ant. 2); third, the square-loop feeding structure with these parasitic square patches and slots (Ant. 3); Finally, based on Ant. 3, four vertical planes are introduced into the proposed antenna. As seen in Figure 3, when four parasitic square patches and slots are etched in the side of the square-loop feeding structure, two AR resonant points are excited at 5.6 and 5.8 GHz, respectively. When combing the square patches with the square slots, the Ant. 3 has good impedance bandwidth and ARBW. However, the IBW and ARBW of the Ant. 3 are not wide enough for wide communication. To improve the IBW and ARBW of the Ant. 3, four vertical planes are introduced into the presented antenna. As seen, the IBW and ARBW of the presented antenna are significantly enhanced compared with Ant. 3. This is because these parasitic patches, slots, and vertical planes could stimulate multiple current flow patches, which excite two CP resonant points. At last, the presented antenna could realize a broad IBW of 4.75–6.75 GHz (34.8%) for $|S_{11}| < -10$ dB and a broad ARBW of 5.04–6.48 GHz (25.0%) for AR < 3 dB.

To study the effects of the antenna sizes on the CP performance, multiple antennas' parameters are scanned, compared, and analyzed in this part. These various parameters consisted of the side length ($L1$) of the square patches, the side length ($L2$) of the square slots, the height ($h1$) of the vertical planes, and the distance ($D1$) of the feeding point. Figure 4 gives the corresponding $|S_{11}|$ and AR results for these parameters. First, the distance ($D1$) of the feeding point has an obvious impact on the AR values because it determines the initial 90° phase difference. Second, the side lengths ($L2$) and height ($h1$) have significant influences on the $|S_{11}|$ and AR results in the whole frequency band. This is because these CP resonant points come from the joint action of the square slots and vertical planes rather than a single action. Moreover, compared with the variations in the other parameters, the length ($L1$) has a dramatic impact on the AR values at high frequencies. The reason is that the role of the square patches is to stimulate an AR resonant point at high frequencies, which is consistent with the results of the step-by-step prototypes in Figure 3. When setting $D1 = 3.0$, $L1 = 12$, $L2 = 12$, and $h1 = 4$ mm, the optimal CP performance could be obtained.

The vector current distributions of the CP MSA on upper and lower surfaces are simulated and plotted in Figure 5, to clarify the CP operating mechanism. As seen, at two AR resonant points (5.35 and 6.35 GHz), the main current and part of the current component with different phases (0° and 90°) are characterized by red and black arrows. First, it is observed that the surface currents are mainly focused on the square patches, the edges of the square slots, and the vertical planes. Second, it can be seen that the total surface currents in the square slots and metal columns are opposite those of the square patches at 5.35 GHz, which would reduce the electrical length and move the operating frequency of the antenna to the higher frequency. Third, it is observed that the total surface currents of square patches and vertical planes are in the same direction and opposite those of the square slots at 6.35 GHz, which would increase the electrical length and move the operating frequency of the antenna to a lower frequency, compared with the results at 5.35 GHz. Finally, the total surface currents of the antenna are orthogonal at 0° and 90° at lower and higher frequencies, respectively. With the variety of phases, the main currents on the antenna rotate anticlockwise at two AR resonant points, which suggests the designed MSA would stimulate the right-hand CP wave in the $+z$ direction.

3. Experimental Results

To prove the accuracy of the design, the designed antenna was simulated, fabricated, and measured in this section.

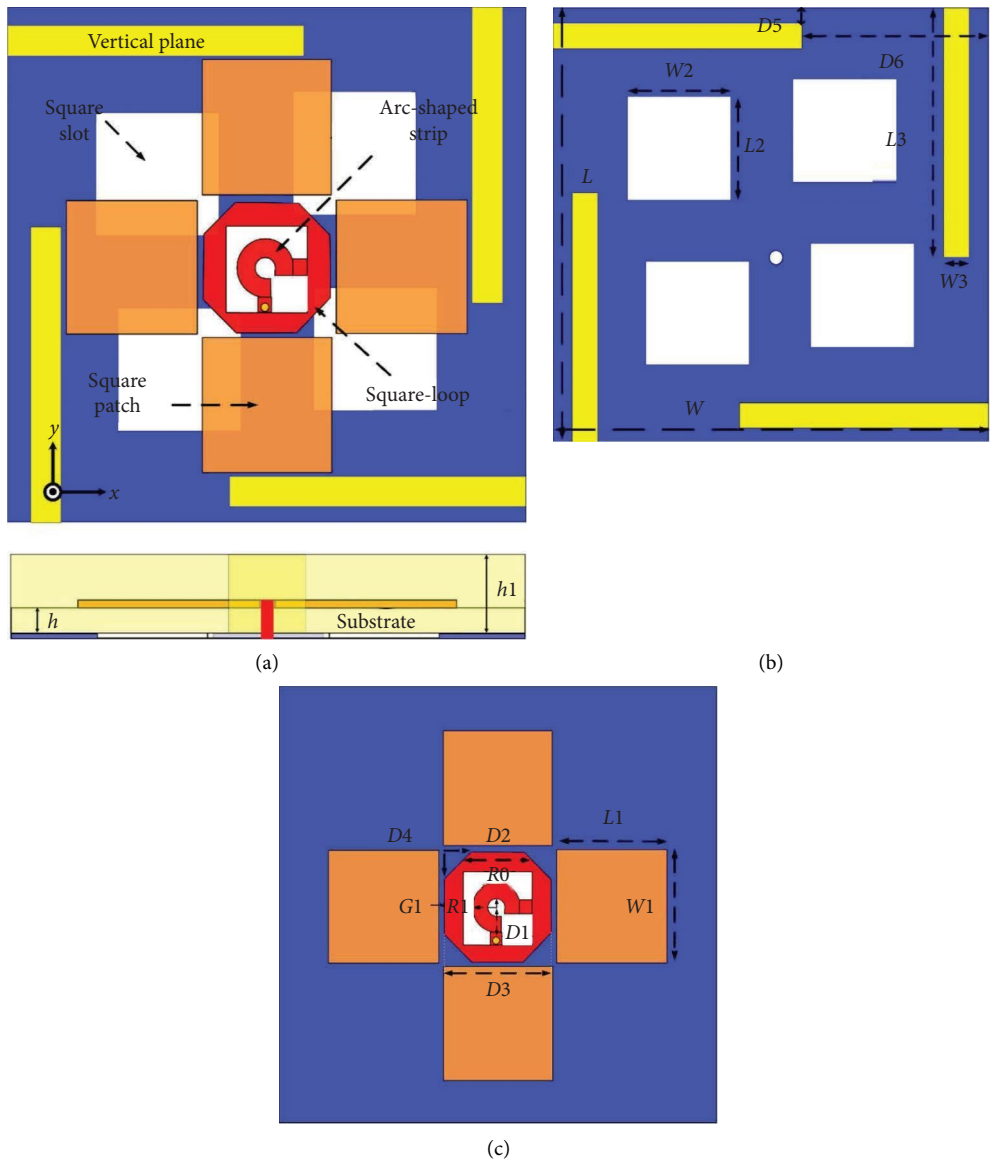

Figure 1: Geometry of the presented CP microstrip slot antenna. (a) The overall structure, (b) the bottom view, and (c) the upper view.

The $|S_{11}|$ value was measured by a vector network analyzer (N5224A), while the radiation pattern, gain, and AR values were measured by the Satimo Starlab Measurement System. Figure 6 gives the simulated and measured $|S_{11}|$ and AR values. As seen, the simulated and measured −10-dB IBW are 34.8% (4.75–6.75 GHz) and 36.4% (4.65 to 6.70 GHz), whereas the 3-dB ARBW are 25.0% (5.04–6.48 GHz) and 25.1% (5.01 to 6.45 GHz), respectively. Further, the simulated and measured CP bandwidths ($|S_{11}| < -10$-dB and AR < 3-dB) are 25.0% (5.04–6.48 GHz) and 25.1% (5.01 to 6.45 GHz). In addition, Figure 7 depicts the measured and simulated gain curves with frequency changes and a photograph of the fabricated antenna. As shown, the measured and simulated peak gains are 10.1 and 9.8 dBi, and the gains gradually increase from low-frequencies to high-frequencies. This is because square slots mainly participate in CP radiation at low frequencies, while square patches participate in that at high frequencies. At last, the simulated and measured radiation pattern values at AR resonant points (4.35, 5.8, and 6.35 GHz) are also shown in Figure 8. It can be seen that the left-hand CP waves are at least 15 dB less than the right-hand CP parts in the *xz*- and *yz*-plane at these AR resonant points, indicating the antenna could excite right-hand CP waves. There is good consistency between the simulation and measurement results. A comparison between the proposed antenna and the recently published CP antennas is shown in Table 2, to

Table 1: Geometrical dimensions of the designed CP MPA.

Parameters	Values (mm)
L	55.4
$L1$	19.2
$L2$	3.0
$L3$	3.0
$D1$	9.2
$D3$	2.4
$D5$	3
$R0$	1.6
h	1.524
W	55.4
$W1$	18.0
$W2$	2.9
$W3$	2.9
$D2$	5.2
$D4$	2.0
$D6$	22
$R1$	3.8
$h1$	4

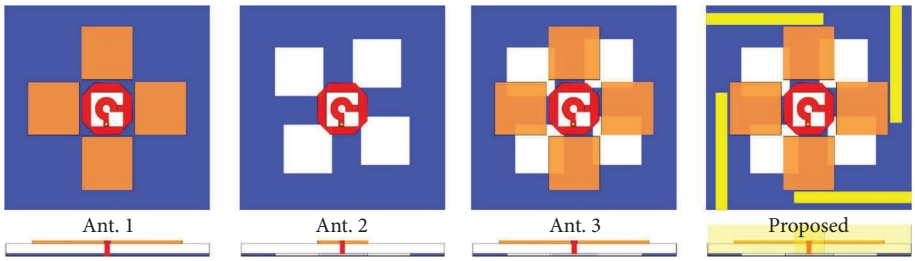

Figure 2: Four step-by-step designed models of the CP MPA.

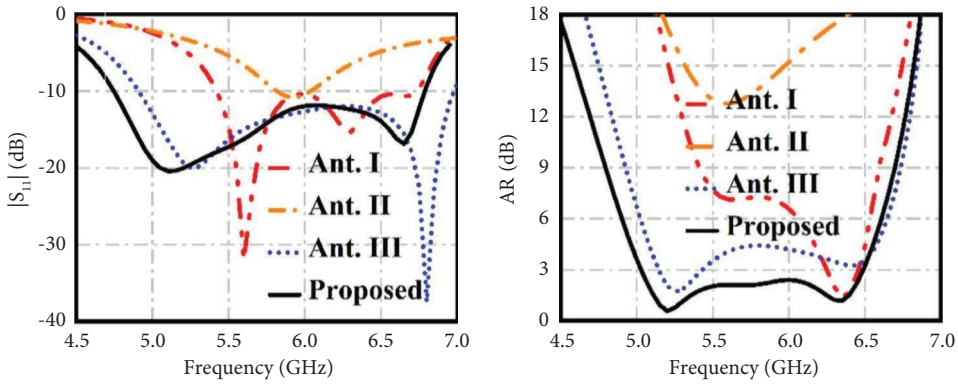

Figure 3: Corresponding $|S_{11}|$ curves and AR curves for different step-by-step antennas. (a) $|S_{11}|$ curves and (b) AR curves.

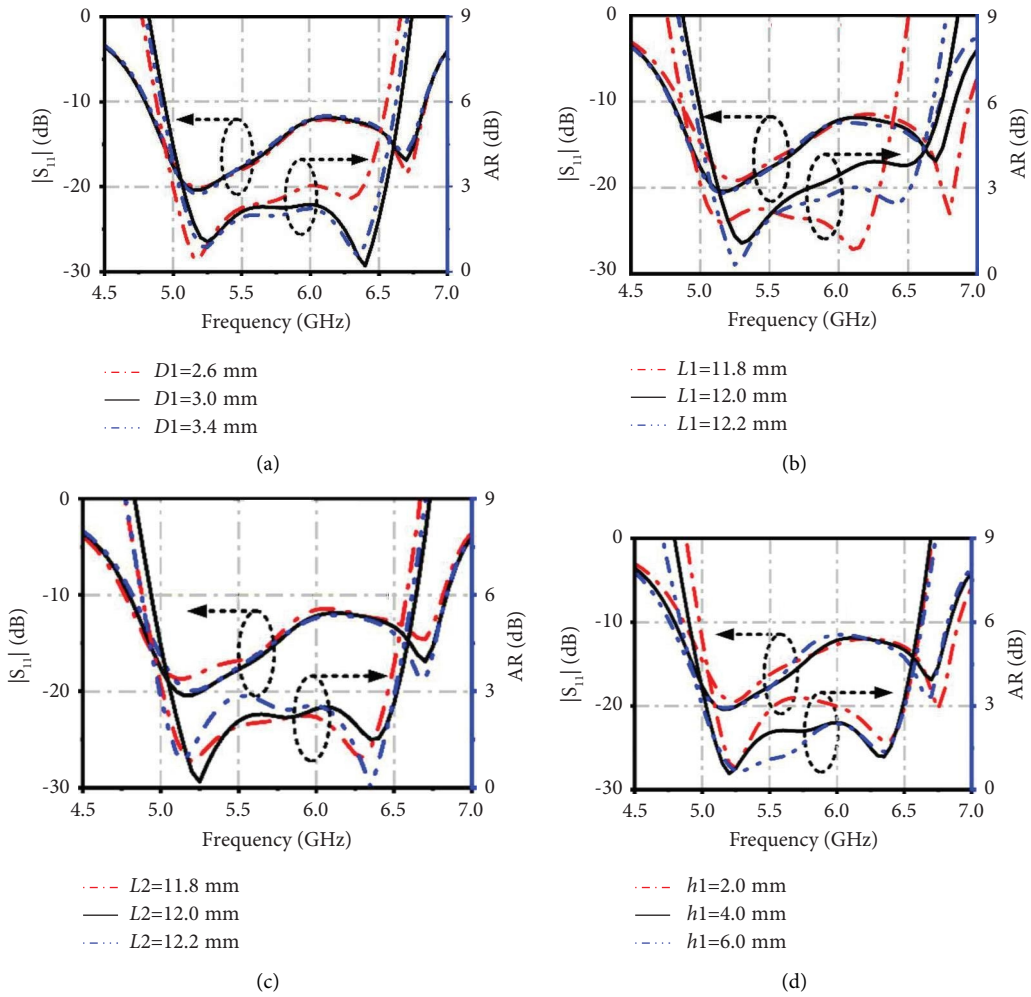

Figure 4: Influence of changing antenna's sizes on the $|S_{11}|$ values and AR values, (a) $D1$, (b) $L1$, (c) $L2$, and (d) $h1$.

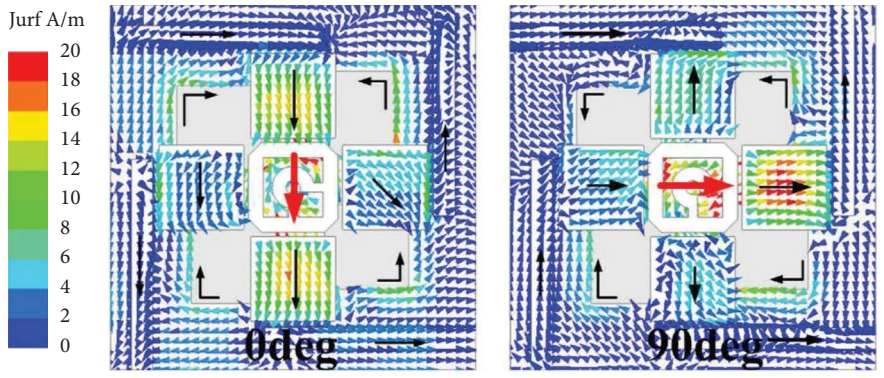

(a)

Figure 5: Continued.

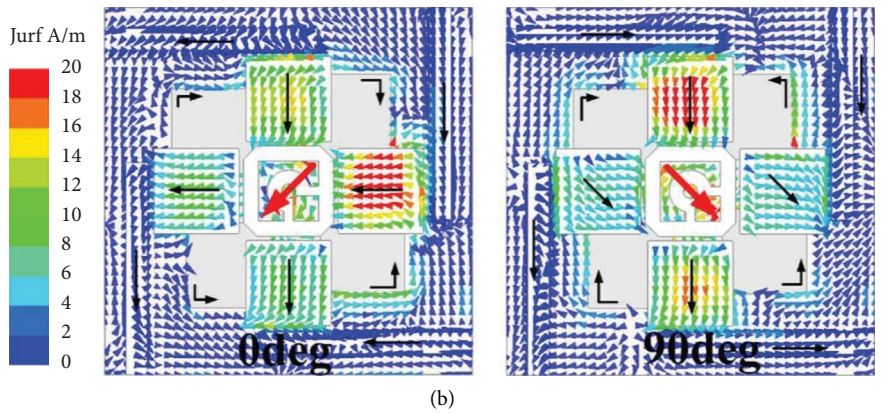

Figure 5: Simulated vector electric field distribution in the CP MSA and its corresponding principal planes with different phases of 0° and 90° at (a) 5.35 GHz and (b) 6.35 GHz, respectively.

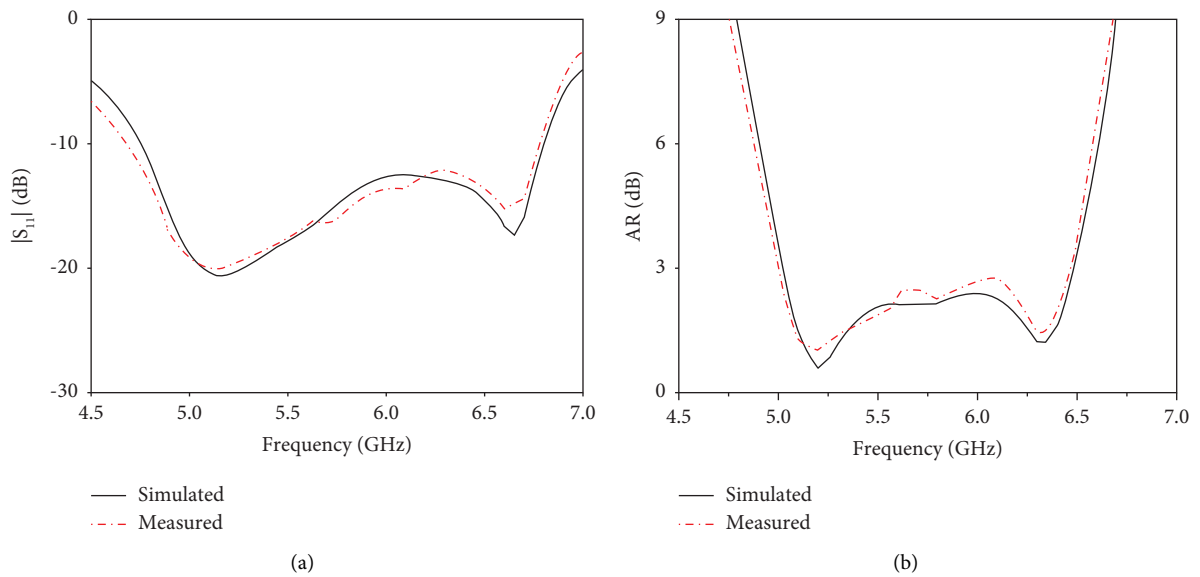

Figure 6: Simulated and measured results with frequencies change. (a) $|S_{11}|$ values and (b) AR curves.

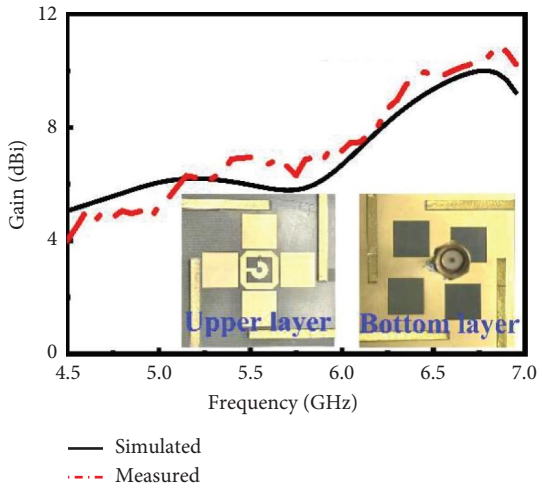

Figure 7: Simulated and measured gain values with frequencies change and the photograph of manufactured antenna.

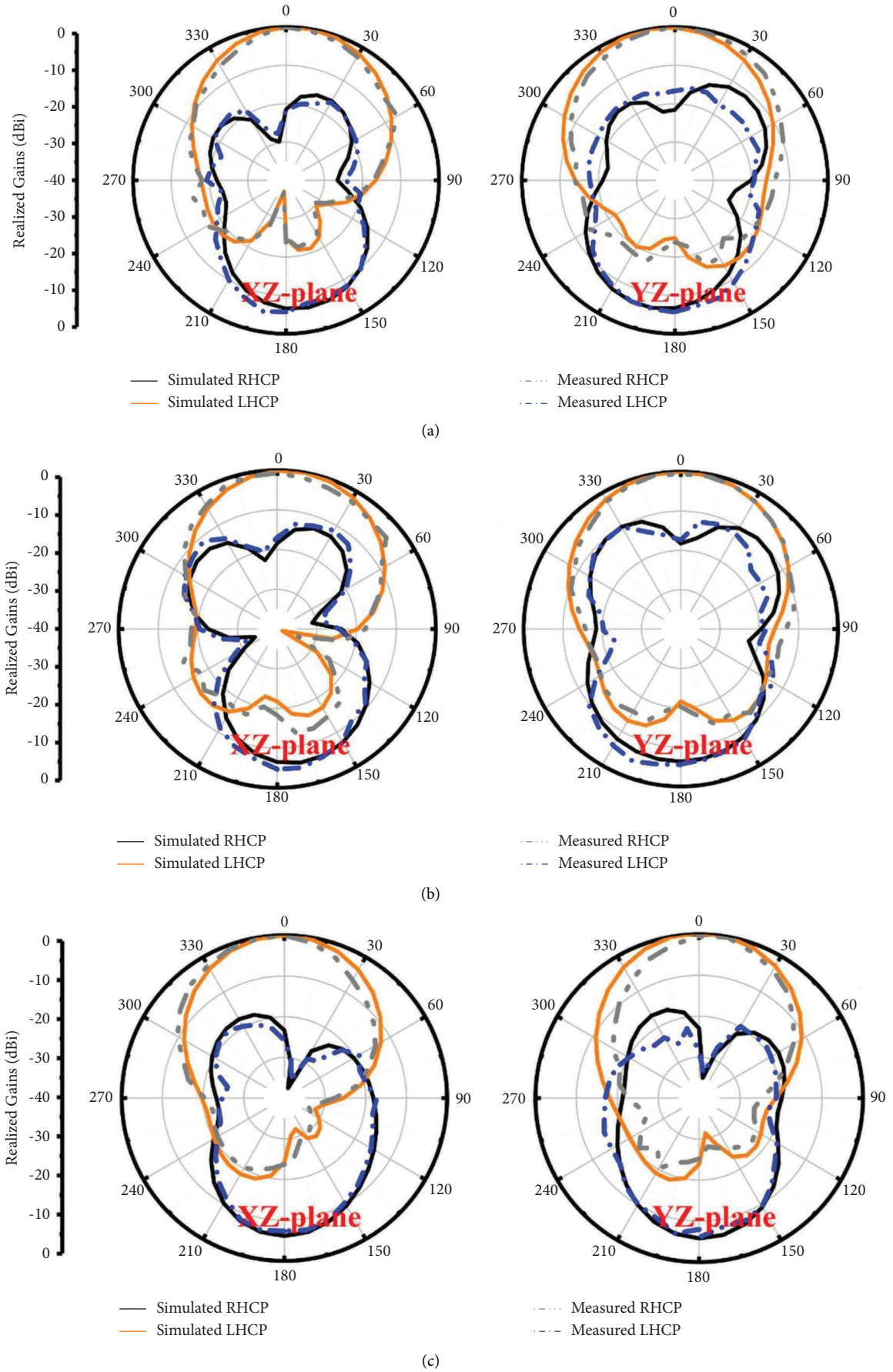

Figure 8: Simulated and measured normalized radiation patterns of the CP MPA at (a) 5.35, (b) 5.80, and (c) 6.35 GHz.

Table 2: Comparison of the designed antenna with previously reported antenna.

Reference Antenna	Type	Antenna size (λ_0^3)	−10-dB IBW (%)	3-dB ARBW (%)	CP bandwidth	Peak gain (dBi)
[13]	Four notched circular-patches + a single-stage transition	$1.16 \times 1.16 \times 0.013$ at 2.5 GHz	8	4.8	4.8	7.5
[15]	Four strips + four rectangular patches + four square-patches	$1.47 \times 1.47 \times 0.028$ at 5.5 GHz	15.8	11.8	11.8	12.5
[37]	Four cut-truncated square-patches + four strip lines	$1.38 \times 1.38 \times 0.028$ at 5.5 GHz	18	12.7	12.7	12
[15]	Four square patches + four parasitic rectangular elements	$1.45 \times 1.45 \times 0.028$ at 5.5 GHz	15.9	11.8	11.8	12.5
[39]	Four cut-truncated square-patches + four square-patches	$0.92 \times 0.92 \times 0.028$ at 5.5 GHz	19.5	12.9	12.9	9.8
[43]	An annular ring + a parasitic circular patch	$0.67 \times 0.67 \times 0.043$ at 0.915 GHz	10.6%	6%	6%	8.9
[44]	A parasitic L-shaped patch + four parasitic square-patches	$0.80 \times 0.80 \times 0.076$ at 5.6 GHz	38	28.1	28.1	8.4
[45]	Four L-shaped patches with L-shaped slots + four square patches + a corner-truncated square patch	$0.95 \times 0.95 \times 0.12$ at 5.6 GHz	25.5	16.7	16.7	10.8
[46]	Eight corner-truncated parasitic square-patches	$0.92 \times 0.92 \times 0.073$ at 5.6 GHz	33.6	19.4	19.4	10.2
Proposed	Four square patches + four square slots + four grounded metal-columns	**$1.03 \times 1.03 \times 0.028$ at 5.6 GHz**	**36.4%**	**25.1**	**25.1**	**10.1**

λ_0 is the free space wavelength at the center frequency of the overlapped band.

demonstrate the advantages of the proposed antenna. The compared results reveal that the proposed antenna has a wider CP bandwidth.

4. Conclusion

In this study, a new stacked microstrip slot antenna (MSA) with wideband circular polarization characteristics is proposed. The antenna consists of a square-loop feed configuration, four parasitic square patches and vertical planes, and a square ground plane etched with four parasitic square slots. These square patches, vertical planes, and square slots as parasitic elements are used to stimulate two CP resonant points. Simulation and measurement are performed on the designed antenna prototype to demonstrate the design's rationality. The measured results depict that the measured impedance bandwidth for $|S_{11}| < -10$ dB is 36.4% (4.65 to 6.70 GHz) and the measured axial ratio bandwidth for AR < 3 dB is 25.1% (5.01 to 6.45 GHz). Compared with other reported stacked CP antennas, the proposed antenna has significant advantages in CP bandwidth, which could occupy the wireless local area network ITS (5.8 GHz), (5.725–5.85 GHz), and WIFI (5.85–5.925 GHz) bands.

Data Availability

The data used to support the findings of this study are available from the corresponding author upon request.

Conflicts of Interest

The author declares that there are no conflicts of interest.

Acknowledgments

This study was supported by GDAS' Project of Science and Technology Development, No.2020GDASYL-20200103120 Special fund project for Enterprise Science and Technology Commissioners of Guangdong Province, No.GDKTP2021020300.

References

[1] U. Patel and T. K. Upadhyaya, "Design and analysis of compact μ-NEGATIVE material loaded wideband electrically compact antenna for wlan/wimax applications," *Progress In Electromagnetics Research M*, vol. 79, pp. 11–22, 2019.

[2] U. Patel and T. K. Upadhyaya, "Dual band planar antenna for GSM and WiMAX applications with inclusion of modified split ring resonator structure," *Progress In Electromagnetics Research Letters*, vol. 91, pp. 1–7, 2020.

[3] U. Patel and T. K. Upadhyaya, "Low profile surface mountable compact microstrip antenna for GPS/WLAN applications," *International Journal of Microwave and Optical Technology*, vol. 16, no. 4, pp. 335–342, 2021.

[4] A. Pandya, T. K. Upadhyaya, and K. Pandya, "Tri-band defected ground plane based planar monopole antenna for Wi-Fi/WiMAX/WLAN applications," *Progress In Electromagnetics Research C*, vol. 108, pp. 127–136, 2021.

[5] A. Pandya, T. K. Upadhyaya, and K. Pandya, "Design of metamaterial based multilayer antenna for navigation/WiFi/satellite applications," *Progress In Electromagnetics Research M*, vol. 99, pp. 103–113, 2021.

[6] T. K. Upadhyaya, R. Pandey, U. P. Patel et al., "Left-Handed material inspired multi-layer planar antenna design for satellite communication applications," *Progress In Electromagnetics Research M*, vol. 108, pp. 201–211, 2022.

[7] A. Vahora and K. Pandya, "Triple band dielectric resonator antenna array using power divider network technique for GPS navigation/bluetooth/satellite applications," *International Journal of Microwave and Optical Technology*, vol. 15, pp. 369–378, 2020.

[8] A. Kumar, K. Saraswat, A. Kumar, and A. Kumar, "Wideband circularly polarized parasitic patches loaded coplanar waveguide-fed square slot antenna with grounded strips and slots for wireless communication systems," *AEU-International Journal of Electronics and Communications*, vol. 114, Article ID 153011, 2020.

[9] A. Kumar, V. Sankhla, J. K. Deegwal, and A. Kumar, "An offset CPW-fed triple-band circularly polarized printed antenna for multiband wireless applications," *AEU-International Journal of Electronics and Communications*, vol. 86, pp. 133–141, 2018.

[10] J. Wang, Y. Li, L. Ge et al., "Millimeter-wave wideband circularly polarized planar complementary source antenna with endfire radiationwith endfire radiation," *IEEE Transactions on Antennas and Propagation*, vol. 66, no. 7, pp. 3317–3326, 2018.

[11] N. Rasool, K. Huang, A. B. Muhammad, and Y. Liu, "A wideband circularly polarized slot antenna with antipodal strips for WLAN and Cband applications," *International Journal of RF and Microwave Computer-Aided Engineering*, vol. 29, no. 11, Article ID e21945, 2019.

[12] G. Li and F.-S. Zhang, "A compact broadband and wide beam circularly polarized antenna with shorted vertical plates," *IEEE Access*, vol. 7, pp. 90916–90921, 2019.

[13] S. K. Lin and Y. C. Lin, "A compact sequential-phase feed using uniform transmission lines for circularly polarized sequential-rotation arrays," *IEEE Transactions on Antennas and Propagation*, vol. 59, no. 7, pp. 2721–2724, 2011.

[14] Y. Li, Z. Zhang, and Z. Feng, "A sequential-phase feed using a circularly polarized shorted loop structure," *IEEE Transactions on Antennas and Propagation*, vol. 61, no. 3, pp. 1443–1447, 2013.

[15] K. Ding, C. Gao, T. Yu, D. Qu, and B. Zhang, "'Gain-improved broadband circularly polarized antenna array with parasitic patches," *IEEE Antennas and Wireless Propagation Letters*, vol. 16, pp. 1468–1471, 2017.

[16] L. Bian and X. Q. Shi, "Wideband circularly-polarized serial rotated 2×2 circular patch antenna array," *Microwave and Optical Technology Letters*, vol. 49, no. 12, pp. 3122–3124, 2007.

[17] L. Wang, W.-X. Fang, W.-H. Shao, B. Yao, Y. Huang, and Y.-F. En, "Broadband circularly polarized cross-dipole antenna with multiple modes," *IEEE Access*, vol. 8, pp. 66489–66494, 2020.

[18] T. K. Nguyen, H. H. Tran, and N. Nguyen-Trong, "A wideband dual cavity-backed circularly polarized crossed dipole antenna," *IEEE Antennas and Wireless Propagation Letters*, vol. 16, pp. 3135–3138, 2017.

[19] S. X. Ta, K. Lee, I. Park, and R. W. Ziolkowski, "Compact crossed-dipole antennas loaded with near-field resonant parasitic elements," *IEEE Transactions on Antennas and Propagation*, vol. 65, no. 2, pp. 482–488, 2017.

[20] J. W. Baik, K. J. Lee, W. S. Yoon, T. H. Lee, and Y. S. Kim, "Circularly polarised printed crossed dipole antennas with broadband axial ratio," *Electronics Letters*, vol. 44, no. 13, pp. 785-786, 2008.

[21] Y. He, W. He, and H. Wong, "A wideband circularly polarized cross-dipole antenna," *IEEE Antennas and Wireless Propagation Letters*, vol. 13, pp. 67–70, 2014.

[22] W. Yang, Y. Pan, S. Zheng, and P. Hu, "A low-profile wideband circularly polarized crossed-dipole antenna," *IEEE Antennas and Wireless Propagation Letters*, vol. 16, pp. 2126–2129, 2017.

[23] L. Wang, Z. Zhu, and Y. En, "Wideband circularly polarized cross-dipole antenna with parasitic metallic cuboids," *International Journal of RF and Microwave Computer-Aided Engineering*, vol. 31, no. 5, Article ID e22572, 2021.

[24] X. Liang, J. Ren, L. Zhang et al., "Wideband circularly-polarized antenna with dual-mode operation," *IEEE Antennas and Wireless Propagation Letters*, vol. 18, no. 4, pp. 767–770, 2019.

[25] L. Zhang, S. Gao, Q. Luo et al., "Single-feed ultra-wideband circularly polarized antenna with enhanced front-to-back ratio," *IEEE Transactions on Antennas and Propagation*, vol. 64, no. 1, pp. 355–360, 2016.

[26] L. Wang, K. Chen, Q. Huang et al., "Wideband circularly polarized cross- dipole antenna with folded ground plane," *IET Microwaves, Antennas & Propagation*, vol. 15, no. 5, pp. 451–456, 2021.

[27] M. Haneishi and Y. Suzuki, "Circular polarization and bandwidth," in *Handbook of Microstrip Antennas*, pp. 220–273, Peregrinus, London, UK, 1989.

[28] P. C. Sharma and K. Gupta, "Analysis and optimized design of single feed circularly polarized microstrip antennas," *IEEE Transactions on Antennas and Propagation*, vol. 31, no. 6, pp. 949–955, 1983.

[29] H. Iwasaki, "A circularly polarized rectangular microstrip antenna using single-fed proximity-coupled method," *IEEE Transactions on Antennas and Propagation*, vol. 43, no. 8, pp. 895–897, 1995.

[30] H. D. Chen, C. Y. D. Sim, and S. H. Kuo, "Compact broadband dual coupling-feed circularly polarized RFID microstrip tag antenna mountable on metallic surface," *IEEE Transactions on Antennas and Propagation*, vol. 60, no. 12, pp. 5571–5577, 2012.

[31] S. Fu, Q. Kong, S. Fang, and Z. Wang, "Broadband circularly polarized microstrip antenna with coplanar parasitic ring slot patch for L-band satellite system application," *IEEE Antennas and Wireless Propagation Letters*, vol. 13, no. 9, pp. 943–946, 2014.

[32] N. Herscovici, Z. Sipus, and D. Bonefacic, "Circularly polarized single-fed wide-band microstrip patch," *IEEE Transactions on Antennas and Propagation*, vol. 51, no. 6, pp. 1277–1280, 2003.

[33] S. M. Kim and W. G. Yang, "Single feed wideband circular polarised patch antenna," *Electronics Letters*, vol. 43, no. 13, pp. 703-704, 2007.

[34] Q. W. Lin, H. Wong, X. Y. Zhang, and H. W. Lai, "Fabricated meandering probe-fed circularly polarized patch antenna with wide bandwidth," *IEEE Antennas and Wireless Propagation Letters*, vol. 13, pp. 654–657, 2014.

[35] Y. Lu, D. G. Fang, and H. Wang, "A wideband circularly polarized 2×2 sequentially rotated patch antenna array," *Microwave and Optical Technology Letters*, vol. 49, no. 6, pp. 1405–1407, 2007.

[36] S. Rahardjo, S. Kitao, and M. Haneishi, "Circularly polarized planar antenna excited by cross-lot coupled coplanar wave guide feedline," in *Proceedings of the International Symposium on Antennas and Propagation*, vol. 3, pp. 2220–2223, Denver, CO, USA, June 1994.

[37] C. Deng, Y. Li, Z. Zhang, and Z. Feng, "A wideband sequential-phase fed circularly polarized patch array," *IEEE*

Transactions on Antennas and Propagation, vol. 62, no. 7, pp. 3890–3893, 2014.

[38] L. Wang, Z. Zhu, and Y. En, "Performance enhancement of broadband circularly polarized slot–microstrip antenna using parasitic elements," *IEEE Antennas and Wireless Propagation Letters*, vol. 20, pp. 2255–2259, 2021.

[39] K. Ding, C. Gao, D. Qu, and Q. Yin, "Compact broadband circularly polarized antenna with parasitic patches," *IEEE Transactions on Antennas and Propagation*, vol. 65, no. 9, pp. 4854–4857, 2017.

[40] K. P. Nasimuddin, K. P. Esselle, and A. K. Verma, "Wideband high-gain circularly polarized stacked microstrip antennas with an optimized C-type feed and a short horn," *IEEE Transactions on Antennas and Propagation*, vol. 56, no. 2, pp. 578–581, 2008.

[41] Z. Wang, S. Fang, S. Fu, and S. Jia, "Single-fed broadband circularly polarized stacked patch antenna with horizontally meandered strip for universal UHF RFID applications," *IEEE Transactions on Microwave Theory and Techniques*, vol. 59, no. 4, pp. 1066–1073, 2011.

[42] L. Wang, L. Fang, X. Zhang, and Y. Chi, "A compact broadband circularly polarized stacked microstrip antenna with parasitic elements," *Radio Science*, vol. 57, no. 6, pp. 1–8, 2022.

[43] X. Chen, G. Fu, S. X. Gong, Y. L. Yan, and W. Zhao, "Circularly polarized stacked annular-ring microstrip antenna with integrated feeding network for UHF RFID readers," *IEEE Antennas and Wireless Propagation Letters*, vol. 9, no. 07, pp. 542–545, 2010.

[44] W. W. Yang, W. Sun, W. Qin, J. Chen, and J. Zhou, "Broadband circularly polarised stacked patch antenna with integrated dual-feeding network," *IET Microwaves, Antennas & Propagation*, vol. 11, no. 12, pp. 1791–1795, 2017.

[45] W. Su, J. Li, and R. Liu, "A compact double-layer wideband circularly polarized microstrip antenna with parasitic elements," *International Journal of RF and Microwave Computer-Aided Engineering*, vol. 31, no. 1, 2020.

[46] K. Ding, "Broadband circularly polarized stacked antenna with sequential-phase feed technique," *IET Microwaves, Antennas & Propagation*, vol. 14, no. 1, pp. 1791–1795, 2020.